Space Science Reviews (2022) 218:24
https://doi.org/10.1007/s11214-022-00891-6

Determining the Relative Cratering Ages of Regions of Psyche's Surface

S. Marchi[1] · E. Asphaug[2] · J.F. Bell III[3] · W.F. Bottke[1] · R. Jaumann[4] · R.S. Park[5] · C.A. Polanskey[5] · T.H. Prettyman[6] · D.A. Williams[3] · R. Binzel[7] · R. Oran[7] · B. Weiss[7] · C.T. Russell[8]

Received: 26 May 2021 / Accepted: 12 April 2022 / Published online: 2 May 2022

Abstract
The study of the cratering history of asteroid (16) Psyche is one of the investigations to be performed by the NASA *Psyche* mission. A dedicated Relative Ages Working Group will carry on these investigations using primarily imaging and topographic data, and complement the interpretation of these data with theoretical models (hydrocodes to simulate impacts) as well as laboratory experiments (impact experiments on relevant target materials). The *Psyche* Science Team will also rely on experience and lessons learned from prior space missions, such as NASA *Dawn* and ESA *Rosetta*.

The main goals of the cratering investigations are to map craters and characterize their morphology across Psyche's surface over a range of spatial resolutions. These data will then be used to constrain relative and absolute ages of Psyche's terrains, and impact-related processes will inform other investigations, such as geological mapping, surface composition, and internal structure. Psyche's cratering data will also be used to perform comparative analyses with similar data from other rocky asteroids. The present chapter provides a pre-launch view of the planned activities and methodologies of the Relative Ages Working Group.

The NASA Psyche Mission: Science Instruments and Investigations
Edited by James F. Bell III, Carol Polanskey and Lindy Elkins-Tanton

✉ S. Marchi
marchi@boulder.swri.edu

1 Southwest Research Institute, Boulder, CO, USA

2 Lunar and Planetary Laboratory, University of Arizona, Tucson, AZ, USA

3 School of Earth and Space Exploration, Arizona State University, Tempe, AZ, USA

4 Institute of geological Sciences, Free University of Berlin, Berlin, Germany

5 Jet Propulsion Laboratory, California Institute of Technology, Pasadena, CA, USA

6 Planetary Science Institute, Tucson, AZ, USA

7 Department of Earth, Atmospheric and Planetary Sciences, Massachusetts Institute of Technology, Cambridge, MA, USA

8 University of California Los Angeles, Los Angeles, CA, USA

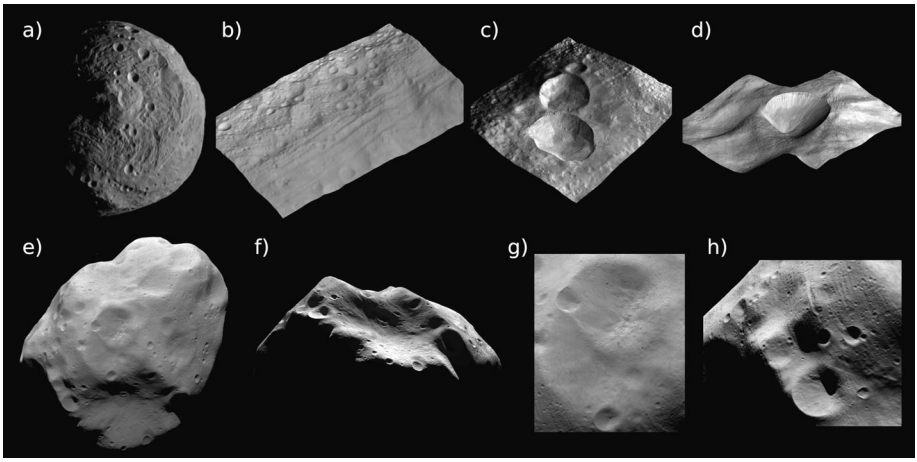

Fig. 1 A summary figure of notable craters on Vesta (**a**-**d**) and Lutetia (**e**-**h**). These asteroids have mean diameters of about 525 and 100 km, respectively, thus bracketing Psyche's size (mean diameter 222 km). **a**) Vesta's southern hemisphere highlighting the Rheasilvia basin, and its central mound; **b**) 3D rendering of Divalia Fossae; **c**) Superposition of craters (the 70-km diameter Marcia crater is the lowest, largest crater in the image); **d**) 17-km diameter Antonia crater, an irregular impact structure located on a steep slope; **e**) Lutetia's irregular shape; **f**) 55-km diameter Massalia crater; **g**) Lutetia's Baetica region sculpted by possibly two or three superposed impacts; **h**) Lutetia's Narbonensis region with throughs and lineaments. Credit: **a**)-**d**) NASA/JPL-Caltech/UCLA/MPS/DLR/IDA; **e**)-**h**) MPS/UPD/LAM/IAA/RSSD/INTA/UPM/DASP/IDA

1 Introduction

Impact cratering is one of the primary processes producing surface modifications on asteroids observed by spacecraft (Marchi et al. 2015, for a review). The largest impacts sculpt the overall shape of asteroids, while smaller impacts excavate and redistribute target material across the surface leading to complex landscapes. The surface spatial density of craters is key to both identify process-specific geologic units as part of geologic mapping, and reconstruct the asteroid's past evolution. In this chapter, we present a brief summary of cratering on notable rocky asteroids, including Vesta and Ceres as revealed by the NASA *Dawn* mission and Lutetia visited by the ESA *Rosetta* mission. The choice to focus on these asteroids is motivated by their bulk properties that are closest to what is currently known about Psyche: Vesta's and Lutetia's sizes bracket that of Psyche and their high densities are similar to Psyche's estimated density (see below). Furthermore, these asteroids share a similar collisional environment, thus facilitating comparative investigations that may help understand target-specific cratering outcomes, for instance due to different material properties. Finally, we note that the *Dawn* and *Psyche* missions have similar observational architectures, therefore the lessons learned from *Dawn* will inform the planning and execution of cratering investigations at Psyche. Additional observations from smaller asteroids (e.g., Eros) will be discussed as relevant.

Vesta's overall geology is the result of impact cratering and its subsequent effects. Two giant impacts (Rheasilvia and Veneneia basins, about 500 and 460 km in diameter, respectively; Marchi et al. 2012a; Schenk et al. 2012) at its south pole altered the original asteroid's ellipsoidal shape (Fig. 1). These impacts excavated crustal and upper mantle material that ended up covering much of the surface, and also was ejected from the asteroid and became the source of the Vesta's asteroid family (Asphaug 1997). Vesta's asteroid family is the

probable source of the howardite, eucrite and diogenite (HED) meteorites reaching Earth (McCord et al. 1970; Russell et al. 2012; McSween et al. 2013; Schenk et al. 2021b). The excavation and deposition of Rheasilvia and Veneneia accounts for much of the topographic structure of Vesta, with a relief of about 42 km (Jaumann et al. 2012; Jutzi et al. 2013). In addition, the energy of these impacts transformed Vesta's surface via impact-induced seismic activity to form tectonic ridge-and-trough systems along the equator and in the northern hemisphere (Divalia and Saturnalia Fossae, respectively; Jaumann et al. 2012; Bowling 2015). Smaller impacts have excavated subsurface materials at multiple locations, including possibly buried volatile-rich materials as a source of localized pitted terrains (as in the 70 km across Marcia crater; Denevi et al. 2012), and igneous intrusions (e.g., Brumalia Tholus, a putative laccolith exposed by Teia crater; Buczkowski et al. 2014). Many localized color variations on Vesta's surface (e.g., Oppia, Octavia craters) appear to represent ejecta from impacts of compositionally distinct material, different from the typical vestan surface (Garry et al. 2014; Williams et al. 2014a). Vesta's bulk density is 3.46 ± 0.01 g/cm^3 (Russell et al. 2012), thus within the range of estimated density for Psyche (Elkins-Tanton et al. 2020, 2021).

Ceres's surface is also largely controlled by cratering (Park et al. 2019, 2020), but there are several notable differences compared to its smaller sibling Vesta. Overall, Ceres' topography has only about 10 km of vertical relief, and it appears to be modulated horizontally by a few large-scale depressions (e.g., Vendimia Planitia, 800 km across) and raised terrains (e.g., Hanami Planum, 560 km across). These depressions are compatible with ancient impact structures, but unlike the Rheasilvia basin on Vesta their origin remains unclear. The largest well-defined impact crater on Ceres is Kerwan (284 km across, Williams et al. 2018), thus highlighting significant depletion of large craters compared to Vesta. Because Vesta and Ceres experienced comparable collision evolution histories over the last 4.5 Gyr or so, this suggests that many large craters on Ceres were not preserved (Marchi et al. 2016), possibly due to its rheologically weak crust that would allow for the gradual removal of complex topography (Fu et al. 2017; Bland et al. 2016; Otto et al. 2019). Ceres' low bulk density ($\sim$2.16 g/cm^3; Russell et al. 2016) indicates a higher volatile content than Vesta, Lutetia and Psyche, and as such Ceres' cratering may not be directly relevant to Psyche. Nevertheless, Ceres is one of the Main Belt asteroids with high resolution coverage and cratering data, therefore it will be useful in comparative analyses.

Important cratering data has also been gathered by other missions. For instance, ESA's *Rosetta* mission flew-by the 100-km asteroid Lutetia, revealing a highly irregular shape sculpted by large craters, such as the 55-km diameter crater Massalia (see Fig. 1). Lutetia's bulk density is 3.4 ± 0.3 g/cm^3 (Sierks et al. 2011). Post-cratering downslope movement of material has also been shown to be an important surface modification process on Lutetia, despite the low surface gravity. For example, Lutetia's Baetica regions show signs of regolith downslope motion on a flank of a possible impact crater, along with a concentration of boulders at the base of the slope (Massironi et al. 2012; Kueppers et al. 2012). Similarly, downslope movement of regolith, and dust transport from impact and solar effects, has created slope streaks, boulder tracks, and flat sedimentary "pond" deposits on the floors of some impact craters on smaller asteroids such as Eros (e.g., Robinson et al. 2001). Eros also revealed a number of tectonic features (Prockter et al. 2002), and a prominent ridge (18-km long Hinks Dorsum) has been interpreted as impact-induced compression due to the formation of Shoemaker crater (Watters et al. 2011). A detailed review of asteroid cratering is beyond the scope of this chapter, and the interested reader is referred to Marchi et al. (2015), and Bottke et al. (2020).

In addition to its other novelties (Elkins-Tanton et al. 2020), Psyche is intermediate in size between Lutetia and Vesta. It will be the first asteroid ever visited in the size range 100-500

km diameter, which may be the size range of the largest asteroids to have been catastrophically disrupted during Solar System history (Bottke et al. 2005), so we can for now only speculate on how global scale (Asphaug et al. 2015) and sub-catastrophic to catastrophic impacts (Holsapple and Housen 2019) will have altered its geology, and on the related question of the absence of a Psyche-derived asteroid family (e.g., Davis et al. 1999).

In addition to space mission data, advanced adaptive optics imaging techniques applied to the largest asteroids are widening the scope of comparative investigations. For example, for the second largest asteroid Pallas (528 km mean diameter), imaging by Marsset et al. (2020) reveal a highly saturated "golf ball" like surface at a scale of about 4 km/pixel. Comparatively, the same technique applied to Psyche by Viikinkoski et al. (2018) achieves a similar spatial resolution but Psyche's reconstructed surface image does not appear crater saturated (see below). It is worth noting Pallas and Psyche are in different collisional environments (e.g., higher average impact velocities for Pallas) and successful recognition of small craters by adaptive optics imaging may be subject to subtle variations in lighting or the crater depth-to-diameter ratios. For example, adaptive optics imaging of Ceres (Vernazza et al. 2020) shows few craters in contrast to findings by the *Dawn* mission, likely due to shallow craters on Ceres compared to Vesta's craters (Schenk et al. 2021a).

This brief summary of the complex nature of large asteroid cratering indicates that the outcome of impact processes is controlled by the asteroid's size, composition, and material properties. Ground-based occultation and high angular imaging resolved Psyche's ellipsoidal shape to have principal axes of 277x238x168 km^3 (222±4 km mean diameter; Ferrais et al. 2020). Uncertainties in volume and mass estimates, result in a density estimate with a most likely range from 3.4 to 4.1 g/cm^3 (Elkins-Tanton et al. 2020). Because of the density and other surface properties, it is thought that Psyche may have a metal content up to 60% (Elkins-Tanton et al. 2020, 2021), and thus cratering may behave in radically different ways compared to rocky asteroids (e.g., Marchi et al. 2020).

It is expected that the gamut of cratering processes described above may play an important role in interpreting Psyche's crater populations. Impact crater abundances are expected to be different on geologic surfaces produced at different times, and thus could be a key referent in determining the relative stratigraphy of Psyche's surface. Craters may also expose materials from the interior of Psyche, or host exogenic materials delivered by comets or asteroids (e.g., water ice in permanently-shadowed regions of worlds like the Moon; e.g., Luchsinger et al. 2021). In addition, the cumulative effects of impacts can add exogenous materials to Psyche's surface over billions of years (e.g., Marchi et al. 2019), and in case of Psyche's high metal content, they could result in complex metal-silicate mixing. Thus, it is anticipated that Psyche's cratering may reveal peculiar traits when compared to previously visited asteroids. Cratering may also lead to the acquisition or modification of remnant magnetization through impact heating or shocks (e.g., Gattacceca et al. 2010). Magnetization of small bodies by impact plasmas has also been proposed (e.g., Muxworthy et al. 2017). Furthermore, determining the relative ages of different regions on the surface may help trace the history of any asteroid-generated dynamo field that may have operated on the body and can now be revealed from the existence of remnant magnetization.

The following sections lay out the *Psyche* Science Team plan to characterize crater populations on Psyche, as informed by pre-launch mission planning and theoretical modeling.

2 Mapping Craters on Psyche

Specific science objectives related to impact cratering have been identified as important goals for the *Psyche* mission to be carried out by the Relative Ages Working Group. In addi-

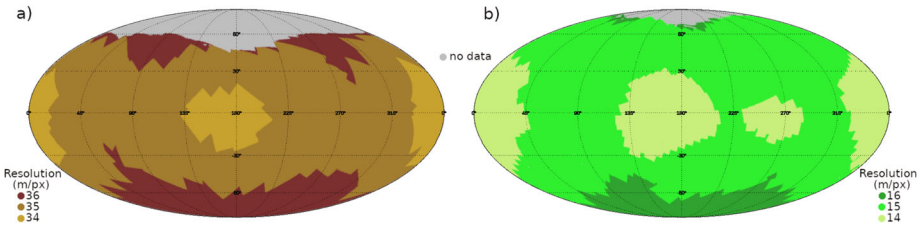

Fig. 2 Mollweide projection of resolution maps for planned observations at Psyche for Orbit A (**a**) and Orbit B (**b**), with an altitude of 700 and 290 km, respectively. Colors indicate the best spatial resolution available and surface coverage. The cumulative area coverage at resolutions higher than 36 m/px (Orbit A) and 16 m/px (Orbit B) is 93% and 98%, respectively. Additional higher resolution imaging of localized areas will be acquired in Orbit C and D (altitude 170 and 85 km, respectively), but with much less surface coverage. Note the gray region near the north pole is not imaged in Orbit A and B, but it will be imaged by Orbit C and D

tion to simply characterizing the overall geology and topography of Psyche at spatial scales of $\leq$ 200 m/pix horizontally and $\leq$ 50 m/pix vertically (Jaumann et al. 2021), these goals also include determining the relative ages of surface regions by counting craters with diameters larger than 1 km over at least 50% of the asteroid. Crater identification and mapping relies on a combination of imaging resolution, coverage and illumination and the mission's cratering objectives are expected to be met using data from the *Psyche* Multispectral Imager investigation (Bell et al. 2021) acquired during a series of increasingly higher-resolution imaging campaigns from lower orbital altitudes over the course of the mission (Polanskey et al. 2021). Comparison with the *Dawn* mission indicates that crater identification can be reliably conducted with 5 pixels per diameter, and possibly down to 3 pixels per diameter under ideal illumination conditions and benign local topography (e.g., smooth terrains as in Marcia crater on Vesta; Marchi et al. 2014). The planned resolution maps are presented in Fig. 2, for the two primary mission phases devoted to imaging (called Orbit A and B). For example, Orbit A (altitude of 700 km) will achieve a resolution of 35 m/px on about 80% of the surface; while in Orbit B (altitude 290 km) will achieve a resolution of 15 m/px on about 90% of the surface, demonstrating that the mission cratering goal of mapping craters larger than 1 km will likely be exceeded (see later for expected crater statistics).

Initial photogeologic analysis of images of Psyche begins with the identification of geologic features, including impact craters. Crater size, shape, morphology (simple, complex, multi-ring structures, etc.) and distribution will be noted, along with identification and mapping the extents of continuous and discontinuous ejecta blankets from impact craters. Identifying contacts between craters and other features and geologic units are essential to determine the stratigraphic history of the asteroid's surface. Cratering data will be obtained primarily using georeferenced images from the Multispectral Imager and derived products, such as mosaics. We will also analyze the topographic data for evidence of large depressions that could represent ancient, degraded impact structures. Here we conveniently discuss specific issues associated with the identification of large and small craters.

Large craters. Psyche's shape is significantly elongated, raising the question of how much of its shape is a byproduct of large impacts. Here we define as "large", those craters with diameter larger than about 1/5th of the asteroid's diameter. Early asteroid investigations showed that the shapes of relatively small asteroids (31-km Ida, 17-km Eros, etc) were primarily controlled by large impacts (e.g., Thomas 1999; Thomas et al. 2002). This conclusion holds true for larger asteroids, and observations of Vesta and Lutetia have shown that large craters are also important to control their overall shape (Fig. 1).

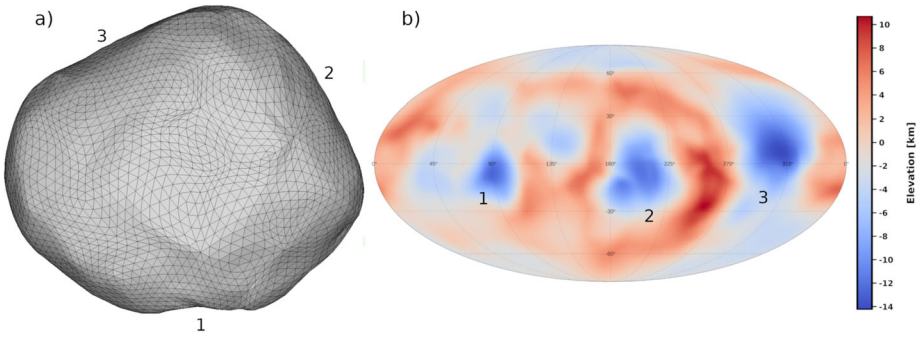

Fig. 3 Psyche shape model and topography. **a**) A polar view of Psyche shape model revealing an equatorial silhouette that largely departs from a regular ellipsoid. Three putative large craters are indicated with 1, 2, 3. **b**) A Mollweide projection of the elevation with respect to the best fit ellipsoid (277x238x168 km^3). The equatorial depressions are indicated. The range of elevation is [−14.2, 10.70] km. Adapted from Ferrais et al. (2020)

On this basis, we expect that large collisions are responsible for some irregularities in Psyche's appearance. A radar shape model (Shepard et al. 2017) shows two distinct depressions, of approximately $\sim$ 67 and $\sim$ 53 km in diameter, which could be impact structures. Viikinkoski et al. (2018) identified two additional depressions $\sim$ 90 km in diameter, while Ferrais et al. (2020) identified three large crater-like depressions larger $\sim$ 44, 60, 80 km in diameter fairly close to Psyche's equator (Fig. 3). Assuming these features are truly impact craters, we might expect they significantly altered Psyche's overall shape and surface properties. The ultimate morphological consequences of these events is a strong function of Psyche's bulk mechanical properties, which remain poorly constrained for the time being. We anticipate, however, that these putative large collisions could have resulted in significant crustal porosity as well as the redeposition of subsurface materials across the Psyche's surface. This may have led to the generation of fine particulates on Psyche's surface. This conclusion holds true also in case of a high metal content for Psyche, as laboratory experiments reveal that cratering in Fe-Ni meteorites and ingots can produce small metal fragments similar to rocky regolith (Marchi et al. 2020; Christoph et al. 2021). In addition, large impacts may also generate widespread tectonic features (ridges, graben, etc.), as proposed for Eros, Ida and Vesta (Buczkowski et al. 2008; Asphaug et al. 1996; Bowling 2015). For Eros, it has been shown that the consecutive formation of the observed three largest craters (Himeros, Psyche, and Shoemaker) could generate up to 20% bulk porosity (Tonge et al. 2016).

While current data provide tantalizing evidence of large craters on Psyche, the extent to which even larger impacts may have been responsible for the Psyche's shape remains to be understood and it is one of the goals of the *Psyche* mission.

Small craters. High resolution imaging of the small crater distribution on Psyche will open a new window in comparative planetology for cratering processes on a wide variety of planetary surfaces. When examined at high resolution in small local regions, Vesta and Lutetia are heavily cratered down to the imaging resolution limit (Fig. 1). Surfaces such as Achaia on Lutetia and Vesta's northern hemisphere are indicative of heavily cratered terrains resulting from the cumulative effect of billion years of collisions (Marchi et al. 2012a,b). These craters are responsible for the gardening of the top layers and therefore may reveal small scale compositional variations resulting from the dredging up of subsurface materials, which may be compositionally distinct from the surface and/or less weathered.

Such processes have been observed on Vesta (Reddy et al. 2012; Pieters et al. 2012), but not on Lutetia, probably because Lutetia appears to be compositionally uniform (Coradini et al. 2011; Masoumzadeh and Boehnhardt 2019). Small craters will also be used for comparative analysis with other smaller asteroids to better constrain cratering processes on bodies with different bulk properties (e.g., Bottke et al. 2020).

3 Synergies Between Cratering and Other Psyche Mission Investigations

It is expected that the Psyche's surface will be heavily cratered at crater sizes smaller than a few km in diameter. The exposure of subsurface materials in recent small impacts may allow for a better characterization of compositional variability across the surface and reveal the presence of crustal stratification (Bell et al. 2021). An interesting and possibly peculiar aspect about Psyche is the interaction of impact-deposited materials (mostly silicates from rocky asteroids) with Psyche's endogenic material which could have high metal content. This situation could lead to metal-silicate mixing resulting in complex surface morphologies and variable composition. Thus, the coupling of cratering and compositional investigations by the Imager and Gamma Ray and Neutron Spectrometer (GRNS) have the potential to disentangle pristine and accreted materials.

As an example, hydrated minerals were found on Vesta's otherwise anhydrous, basaltic surface (De Sanctis et al. 2012; Prettyman et al. 2012; McCord et al. 2012; Reddy et al. 2012). Hydrated species, thought to result from the infall of carbonaceous chondrite impactors, were most abundant in more heavily cratered regions containing basaltic rock types representative of Vesta's ancient crust (e.g., McSween et al. 2013; Ammannito et al. 2013; Prettyman et al. 2013). Moreover, a portion of the dark material may have been emplaced as ejecta from the impact that formed the Veneneia basin, which is overlain by the younger Rheasilvia basin in Vesta's southern hemisphere (e.g., Reddy et al. 2012; Turrini et al. 2014). As such, the distribution of hydrated minerals provides information on Vesta's chronostratigraphy. Based on telescopic observations in the near-IR, Psyche too is thought to be contaminated with water/OH-bearing minerals (Takir et al. 2016). Consequently, measurements of hydrogen by Psyche's GRNS (Lawrence et al. 2021) may provide additional information on the timing, flux and makeup of the impactors.

In addition, Psyche's reflectance spectra have been interpreted as a metal powder mixture with up to 10 wt.% orthopyroxenes (e.g., Ockert-Bell et al. 2010; Fornasier et al. 2010; Hardersen et al. 2011), although this interpretation is not unique. Interestingly, spatial heterogeneities in surface properties have been proposed based on optical, radar and ALMA data (Shepard et al. 2021; de Kleer et al. 2021). Lacking detailed information about the spatial distribution of the silicate component (e.g., intimate vs areal mixing) it is not clear if these silicates are the result of impact contamination. Spatially resolved color data by Psyche's imager could provide further insight on the origin of the silicate component (Bell et al. 2021).

One of the primary objectives of the Psyche mission is determining whether the asteroid carries remnant magnetization that could be a record of a past dynamo (Elkins-Tanton et al. 2021). There are three possible synergies between the study of cratering processes and the magnetometry investigation. These all relate to the central goal of the magnetometry investigation to characterize the magnetization in Psyche to understand the asteroid's thermal evolution and the history of past magnetic fields (Weiss et al. 2021). First, combining information about the ages of different regions with their inferred magnetization could constrain

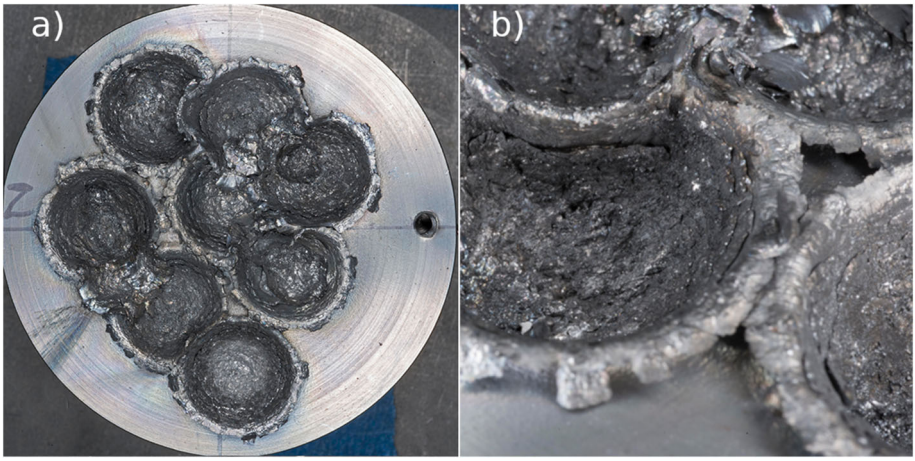

Fig. 4 Consecutive impacts on a Fe-Ni ingot with a diameter of 7 cm (**a**), and close up views of interesting features (**b**). The petal structure of adjacent craters interact to form a complex intersecting pattern, while the superposition of craters produces a large topographic excursion. The 13 superposed craters were produced by silica impactors with diameters of 3.175 and 6.35 mm, and impact velocities ranging from 4.5–5.5 km/s. Adapted from Marchi et al. (2020)

temporal changes in the core dynamo field. Second, because impact processes may heat, shock, and/or fracture, they can affect the magnetization in the body. If a field is present during an impact, this can lead to the acquisition of thermal or shock remnant magnetization of basin and ejecta materials. Alternatively, if no field is present, impact heating and shock can lead to demagnetization. Lastly, impact in the presence of a dynamo could generate plasmas that modify the dynamo field (Hood and Artemieva 2008; Oran et al. 2020). However, studies of how impacts may modify an ambient field and whether such a modified field could magnetize crustal rocks have so far been limited largely to the Moon and other rocky bodies (Chen et al. 1995; Hood and Artemieva 2008; Weiss et al. 2010; Oran et al. 2020). Revealing the magnetic history of Psyche may therefore benefit from crater chronology while also potentially being complicated by the contemporaneous processes of dynamo evolution, impact cratering, and thermal evolution.

Another aspect of interest is the interaction between topography and crater morphology. As discussed above, cratering is sensitive to material properties. The possible metal-rich nature of Psyche may result in interesting crater morphologies. Laboratory impact experiments in iron meteorites and Fe-Ni ingots have shown that craters exhibit sharp rims that retain a competent structure, as opposed to cratering in rocks (Libourel et al. 2019; Marchi et al. 2020). Also, crater floors are characterized by the presence of concentric segments, resembling somewhat the structure of rose petals. These craters have a typical depth-to-diameter ratio of ~ 0.4, compared to 0.15-0.25 for rocky targets (Marchi et al. 2020, and references therein). Processes such as cracking and spallation are also less frequent owing to the high strength of metals, implying that a metallic surface can retain more craters per unit area (Fig. 4). We stress that these peculiar crater morphologies observed in metal targets are dominated by the material strength, and their applicability to larger craters is unclear (see below).

Furthermore, available topography data reveal Psyche's complex topography with a global vertical excursion in excess of 20 km (Fig. 3b). This could generate locally steep slopes, thus resulting in asymmetric craters such as those observed on Vesta and Lutetia

(Massironi et al. 2012; Marchi et al. 2012a; Jaumann et al. 2012; Krohn et al. 2014; Fig. 1). The morphology of craters may also inform us about subsurface inhomogeneities, such as void spaces resulting from fracturing or a rubble pile structure. Interestingly, the presence of significant macroporosity could account for Psyche's reduced density compared to iron meteorites (Elkins-Tanton et al. 2020; Marchi et al. 2020). Under these circumstances, it is expected that craters with sizes comparable with average block size or fracturing spacing would have irregular, polygonal shapes. Similar explanations have been proposed for irregular craters on Vesta and Ceres (e.g., Schenk et al. 2021a). See Jaumann et al. (2021), for further details.

4 Crater Chronologies for Main Belt Asteroids

As outlined in the previous section, cratered landscapes provide valuable insights in the overall geological evolution and physical properties of asteroids. In addition, crater statistics is a powerful tool to interpret the temporal evolution of the surface. In general, higher crater spatial densities imply older terrains. This simple observation constitutes the basis of chronostratigraphic analyses (see next section). Here we will discuss the basic principles of crater formation and interpretation of crater spatial densities.

The crater size is a complex function of impactor size, mass, velocity, and the mechanical properties of the target. Simplified analytical expressions have been derived (e.g., Holsapple and Housen 2007) to better understand how to turn these parameters into craters of a given size. The so-called Pi-scaling law allows computation of the transient crater diameter (D_t) as a function of impactor size (d), impact conditions and material properties, and reads:

$$D_t = kd\left[\frac{gd}{2v_\perp^2}\left(\frac{\rho}{\delta}\right)^{2\nu/\mu} + \left(\frac{Y}{\rho v_\perp^2}\right)^{(2+\mu)/2}\left(\frac{\rho}{\delta}\right)^{\nu(2+\mu)/\mu}\right]^{-\mu/(2+\mu)} \quad (1)$$

where g is the target gravitational acceleration, $v_\perp$ is the perpendicular component of the impactor velocity, δ is the projectile density, ρ and Y are the density and "cratering strength" of the target, k and μ depend on the cohesion of the target material and ν on its porosity. Therefore, the nature of the terrain affects the crater efficiency and the functional dependence of the crater size with respect to the input parameters (e.g., impactor size and velocity).

A critical parameter is target cratering strength. This is an empirical quantity associated with but not equivalent to material tensile-shear strength, and it is particularly important for small craters, which form in the so-called strength regime. The effects of material strength are negligible in larger collisions, which are solely controlled by the target's gravity. This is supported by numerical modeling of the largest craters on Vesta (Jutzi and Asphaug 2015) show an increased influence of material friction at these sizes, further complicating the analysis, but indicating that the largest craters are roughly as predicted by gravity scaling.

Although it is not expected to be abrupt, a transition from strength to gravity dominance is where the left and right terms inside the brackets of Eq. (1) are equal, i.e. impactor diameter d_{sg}:

$$d_{sg} = 2\frac{v_\perp^2}{g}\left(\frac{Y}{\rho v_\perp^2}\right)^{(2+\mu)/2}\left(\frac{\rho}{\delta}\right)^{\nu} \quad (2)$$

Equation (1) provides the so-called transient crater size resulting from the direct excavation and removal of target material. Large craters on planetary surfaces are expected to

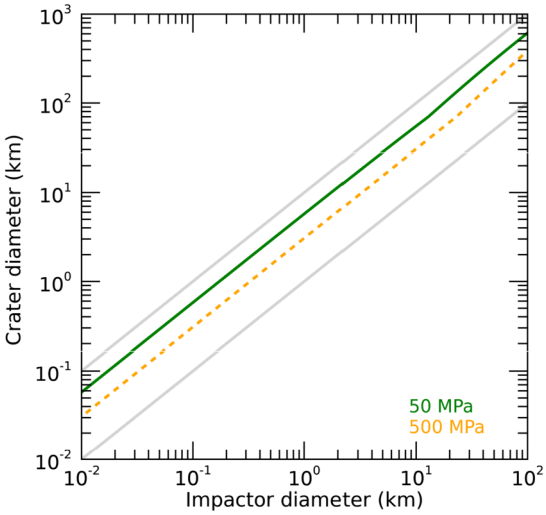

Fig. 5 Final crater size vs impactor size as a function of target strength (as indicated). The chosen strength values are representative values for metal-rich targets (see text). For reference, the gray lines correspond to $D_f = d$ and $D_f = 10d$

undergo a phase of crater modification in which highly fractured materials flow back toward the cavity. The resulting final crater (D_f) is typically from 20% to 50% larger than the transient crater in rocky targets. The modification stage is expected to suppress some of the peculiar crater morphologies observed in laboratory impacts on metallic targets. Figure 5 shows the computed crater size vs impactor size for average impact velocity at Psyche. It is interesting to use Eq. (2) to calculate the impactor diameter corresponding to the transition from strength to gravity regime. Using $Y = 50$ MPa (see below for more details) and a computed average impact velocity for Psyche of 3.7 km/s (so the vertical component is 2.6 km/s), $d_{sg} \sim 40$ km, and $D_f > 200$ km. This indicates that cratering on Psyche may be largely dominated by the strength regime. If correct, this prediction would have important consequences as it indicates that crater morphology is controlled by target strength making the morphologies observed in small-scale laboratory experiments more relevant.

If the asteroid has uniform properties across the surface, the spatial density of small craters superposed on different terrains can be used to infer relative age. In reality, however, this may not be the case. Consider for instance a scenario in which Psyche's surface has metal-rich and silicate-rich terrains. If the two terrains have the same age, we expect a similar total number of impacts, yet craters in the metal-rich terrain would be systematically smaller than in the silicate-rich terrain. Therefore, at a given crater size, it would appear that the metal-rich terrain has less craters. This may erroneously suggest these terrains are considerably younger than the silicate-rich terrains.

Craters are also subject to erasure processes. This is obviously the case when consecutive impacts occur in the same location. Older craters can be totally or partially removed by a younger impact, depending on their relative sizes. Craters can also be eroded by ballistic emplacement of ejecta from distant impacts, or slope failure due to seismic shaking (O'Brien et al. 2006; Richardson 2009; Minton et al. 2019). These processes have been modeled for certain rocky asteroids (e.g., Marchi et al. 2015 for a review) and their applicability to Psyche remains to be investigated.

In order to assess the crater production rate on a given asteroid surface, we need several quantities: the collision probabilities and impact velocities between the target asteroid and the Main Belt population, a crater scaling law that can turn projectiles into craters (or vice

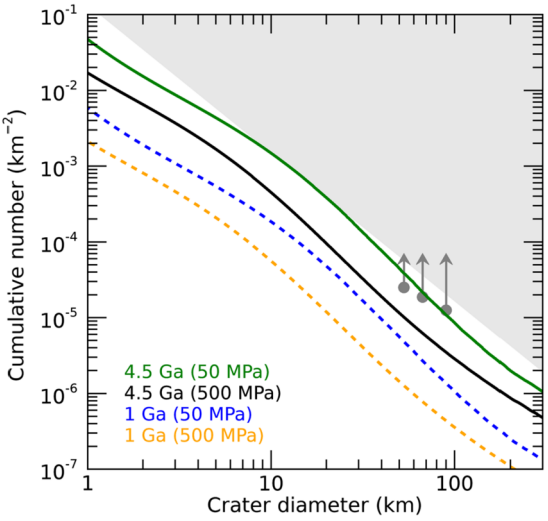

Fig. 6 Psyche's cratering models. The curves indicate the model production functions for the anticipated cumulative number of craters for different strength values and terrain ages, as indicated. The model neglects crater erasing. The data points indicate the four independent large-scale cavities (putative impact craters) inferred from ground-based data (see text). The shaded area indicates crater saturation (the lower bound is 10% of the geometric saturation, as commonly used for rocky terrains)

versa), and the physical properties of the target body. We demonstrate this here by creating a test model of crater production on Psyche.

We use Eq. (1) in its general formulation (including the strength to gravity regime transition) as our crater scaling law for this exercise ($\mu = 0.55$; $\nu = 0.4$). We adopt a Psyche bulk density of 4.1 g/cm^3, a mean diameter of 222 km (Ferrais et al. 2020) and an impactor density of 2.6 g/cm^3. This latter value is an approximation, given that Main Belt projectiles have a variety of compositions and bulk densities. We computed the asteroid impact velocity distribution for Psyche by considering asteroids larger than 50 km in diameter crossing Psyche's orbit (see Marchi et al. 2012b, 2016), obtaining an average value of 3.7 km/s and an intrinsic probability of collision of 4.13×10^{-18} km^{-2} yr^{-1}. We also adopted an impactor size-frequency distribution from the Main Belt evolution model of Bottke et al. (2020). We considered two cratering strength values for illustrative purposes: 500 MPa (for solid metal; Marchi et al. 2020); and a reduced strength of 50 MPa more appropriate if Psyche is heavily fractured and/or contains a significant fraction of silicates, perhaps as indicated by its inferred bulk density (Elkins-Tanton et al. 2020). For reference, intact basalt has a strength of 20 MPa (e.g., Cotto-Figueroa et al. 2016). Finally, we implemented a correction for transient-to-final crater $D_f = 1.3 D_t$, as typically done for rocky targets, but we note that the validity of this correction is questionable for a metallic target.

The resulting model production functions (MPFs), that is the computed number of craters per unit surface for 4.5 and 1 Ga, and for two values of strength, are reported in Fig. 6. The data points indicate the inferred crater cumulative numbers corresponding to the four large cavities larger than 50 km in diameter. This is likely a lower limit of the real number of large craters (as indicated by the vertical arrows). This analysis indicates that if Psyche's strength is close to 500 MPa, then the putative large craters would be very old. Conversely, a greater number of large craters on Psyche would imply that the strength has to be significantly lower than ~500 MPa. Therefore, the number of large craters on Psyche is expected to provide an important constraint on the bulk strength, and its putative metallic nature.

The MPFs are a tool to assess the number of small craters as a function of time. For instance, for a Psyche surface of 1 Ga, it is expected to have between 5 to 30 craters larger than 10 km, or between 500 and 3,000 craters larger than 1 km, depending on the target strength. The number of craters could be significantly higher if the target strength were

lower than assumed in the models presented in Fig. 6. Even in the case of higher strength, we expect the statistics of craters coupled with surface coverage (see Sect. 2) would allow us to perform robust comparative statistical analysis on units across the surface.

Furthermore, craters cannot accumulate indefinitely due to erasure, as discussed in the previous section. For rocky objects such as the Moon and Vesta, the theoretical crater saturation limit is often referred to as 10% of the geometrical saturation for closely packed craters (e.g., Marchi et al. 2012b; Fig. 6). This would translate in a total number of craters larger than 1 km over Psyche's surface of $\sim 10^4$. Thus, the actual number of craters larger than 1 km observed on Psyche could provide an indirect constraint on the terrain strength: if a small number of 1 km craters (close to 500, as noted above) is observed and no obvious sign of recent erasure is found, then the strength of the terrains is metal-like.

5 Toward a Chronostratigraphy for Psyche

Mapping impact crater abundances and distributions are an essential part of geologic mapping of planetary surfaces. Identifying contacts between craters and other features and geologic units are essential to determine the stratigraphic history of the asteroid's surface. In particular, we will be looking for impact crater distributions on homogeneous units, i.e., surfaces that have morphological, compositional, or topographic attributes indicative of being formed by a temporally-distinct process or set of geologic processes. In general, for a given set of geologic units, the greater the number of craters on the unit, the older the unit. Older units also have a great abundance of larger diameter craters compared to younger units. All impact craters down to a given diameter limit (based on image resolution) in a given unit are mapped and plotted in a size-frequency distribution graph, and comparison of these graphs aids in determination of the relative ages of the surface units.

Additionally, by applying established impact crater chronology functions to these size-frequency distributions (e.g., the MPFs presented in the previous section), it is possible to derive absolute model ages for each geologic unit or area in which craters have been counted. These absolute model ages, typically reported in million or billions of years old, provide a numerical referent for comparison of times of geologic activity on Psyche, that can be compared with other objects in the Solar System. Application of crater statistical methods to age date planetary surfaces has been well established (Arvidson et al. 1978). For example, during the geologic mapping of Vesta, identification of the largest impact events, and recognition of geologic units produced by those events, were essential to develop a chronostratigraphy and geologic time scale for that asteroid. Specifically, the two largest south polar impact craters, Veneneia and Rheasilvia, were used to demarcate the bulk of Vesta's geologic history: Pre-Veneneian Period, the oldest crustal material, ~2-4.6 Ga; Veneneian Period, the materials produced between the Veneneia and Rheasilvia impact events, ~1-2 Ga; and Rheasilvian Period, the materials produced by the Rheasilvia impact, $\lesssim$ 1 Ga. A final period, Marcian, was added for one of the youngest large craters, ~200-390 Ma to present (Fig. 7; Williams et al. 2014a,b).

A similar approach will be developed for asteroid Psyche. Global mosaics and topography maps will be used to produce a global geologic map. This map, in which variations in albedo, morphology, roughness, topography, color (composition), and crater abundances will be used to define and characterize geologic units indicative of the geologic processes that formed them, will enable identification of the major, global-affecting processes that will define major units suitable for a stratigraphy system. Lithostratigraphic units will be used to determine chronostratigraphic units, and the corresponding chronology units that will define Psyche's geologic time scale (Williams et al. 2014a).

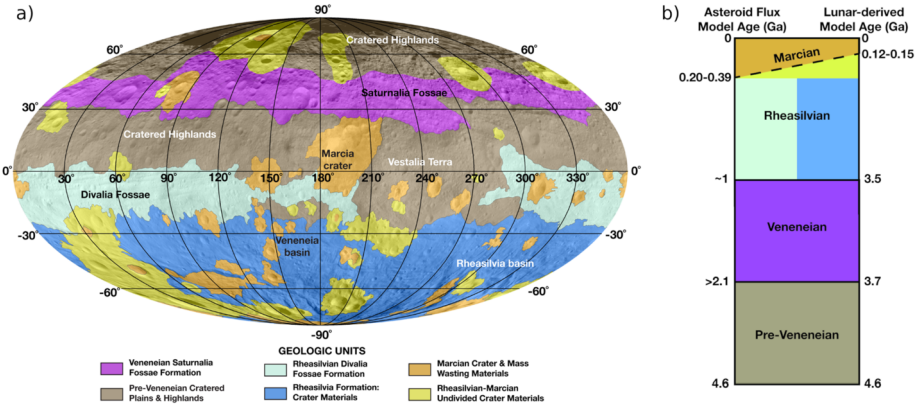

Fig. 7 Mollweide projection of a simplified global geologic map of asteroid Vesta (**a**) consistent with global chronostratigraphy and (**b**) geologic time scale. Adapted from Williams et al. (2014a)

6 Conclusions

In this chapter we presented the planned activities of the *Psyche* mission Relative Ages Working Group and associated cratering studies. Craters are expected to be a primary evolutionary process for Psyche's surface, as indicated by prior studies of asteroids. However, the outcome of impacts on Psyche could radically differ from rocky siblings. If Psyche has a high metal abundance, for instance, craters could have different morphologies than on other rocky bodies. Processes associated with impacts, such as fracturing and generation of fine particulates, could also be different from rocky asteroids, as revealed by laboratory impact experiments on iron meteorites. The presence and number of large craters coupled with Main Belt collisional models will provide important constraints on the bulk properties of Psyche. Smaller craters may be used to derive relative ages of different geological units, and provide absolute cratering age. Relative and absolute ages will be used to derive a chronostratigraphy of Psyche surface in conjunction with geological mapping.

The activities of the Relative Ages Working Group will be carried on synergistically with those of the other working groups as outlined in several chapters in this book. In particular, it is expected that impact-related processes affect topography (Jaumann et al. 2021), internal structure (Zuber et al. 2021), surface composition (Lawrence et al. 2021; Bell et al. 2021), and magnetization history (Weiss et al. 2021). Thus, the products derived by the Relative Ages Working Group (e.g., crater catalogs) will be distributed and utilized by the whole *Psyche's* Science Team to carry on the mission scientific objectives.

References

E. Ammannito, M.C. De Sanctis, F. Capaccioni, M. Teresa Capria, F. Carraro, J.-P. Combe, S. Fonte, A. Frigeri, S.P. Joy, A. Longobardo, G. Magni, S. Marchi, T.B. McCord, L.A. McFadden, H.Y. McSween, E. Palomba, C.M. Pieters, C.A. Polanskey, C.A. Raymond, J.M. Sunshine, F. Tosi, F. Zambon, C.T. Russell, Vestan lithologies mapped by the visual and infrared spectrometer on Dawn. Meteorit. Planet. Sci. **48**, 2185–2198 (2013). https://doi.org/10.1111/maps.12192

R. Arvidson, J. Boyce, C. Chapman, M. Cintala, M. Fulchignoni, H. Moore, G. Neukum, P. Schultz, L. Soderblom, R. Strom, A. Woronov, R. Young, Standard techniques for presentation and analysis of crater size-frequency data. Icarus **37**, 467–474 (1978)

E. Asphaug, Impact origin of the Vesta family. Meteorit. Planet. Sci. **32**, 965–980 (1997). https://onlinelibrary.wiley.com/doi/abs/10.1111/j.1945-5100.1997.tb01584.x

E. Asphaug, J.M. Moore, D. Morrison, W. Benz, M.C. Nolan, R.J. Sullivan, Mechanical and geological effects of impact cratering on Ida. Icarus **120**, 158–184 (1996)

E. Asphaug, G. Collins, M. Jutzi, Global scale impacts, in *Asteroids IV* (2015), pp. 661–678

Bell et al. (2021). This book

M.T. Bland, C.A. Raymond, P.M. Schenk, R.R. Fu, T. Kneissl, J.H. Pasckert, H. Hiesinger, F. Preusker, R.S. Park, S. Marchi, S.D. King, J.C. Castillo-Rogez, C.T. Russell, Composition and structure of the shallow subsurface of Ceres revealed by crater morphology. Nat. Geosci. **9**, 538–542 (2016). https://doi.org/10.1038/ngeo2743

W.F. Bottke Jr., D.D. Durda, D. Nesvorný, R. Jedicke, A. Morbidelli, D. Vokrouhlický, H.F. Levison, Linking the collisional history of the main asteroid belt to its dynamical excitation and depletion. Icarus **179**(1), 63–94 (2005)

W.F. Bottke, D. Vokrouhlický, R.-L. Ballouz, O.S. Barnouin, H.C. Connolly, C. Elder, S. Marchi, T.J. McCoy, P. Michel, M.C. Nolan, B. Rizk, D.J. Scheeres, S.R. Schwartz, K.J. Walsh, D.S. Lauretta, Interpreting the cratering histories of Bennu, Ryugu, and other spacecraft-explored asteroids. Astron. J. **160**, 14 (2020). https://doi.org/10.3847/1538-3881/ab88d3

T.J. Bowling, Global surface modification of Asteroid 4 Vesta following the Rheasilvia impact. Thesis (Ph.D.)–Purdue University (2015); Publication Number: AAT 3736753; ISBN: 9781339256887; Source: Dissertation Abstracts International, Volume: 77-04(E), Section: B.; 174 p.

D.L. Buczkowski, O.S. Barnouin-Jha, L.M. Prockter, 433 Eros lineaments: global mapping and analysis. Icarus **193**, 39–52 (2008). https://doi.org/10.1016/j.icarus.2007.06.028

D.L. Buczkowski, D.Y. Wyrick, M. Toplis, R.A. Yingst, D.A. Williams, W.B. Garry, S. Mest, T. Kneissl, J.E.C. Scully, A. Nathues, M.C. De Sanctis, L. LeCorre, V. Reddy, M. Hoffmann, E. Ammannito, A. Frigeri, F. Tosi, F. Preusker, T. Roatsch, C.A. Raymond, R. Jaumann, C.M. Pieters, C.T. Russell, The unique geomorphology and physical properties of the Vestalia Terra plateau. Icarus **244**, 89–103 (2014). https://doi.org/10.1016/j.icarus.2014.03.035

G. Chen, T.J. Ahrens, R. Hide, Hypervelocity impacts and magnetization of small bodies in the Solar System. Icarus **115**(1), 86–96 (1995)

J.M. Christoph, T. Sharp, S. Marchi, L.T. Elkins-Tanton, Characterizing ejecta fragments from impact experiments into meteoric iron using Scanning Electron Microscopy (SEM), in *52nd Lunar and Planetary Science Conference*, held virtually, 15–19 March, 2021, LPI Contribution No. 2548, id. 2730

A. Coradini, F. Capaccioni, S. Erard et al., The surface composition and temperature of asteroid 21 Lutetia as observed by Rosetta/VIRTIS. Science **334**(6055), 492 (2011)

D. Cotto-Figueroa, E. Asphaug, L.A.J. Garvie, A. Rai, J. Johnston, L. Borkowski et al., Scale-dependent measurements of meteorite strength: implications for asteroid fragmentation. Icarus **277**, 73–77 (2016)

D.R. Davis, P. Farinella, F. Marzari, The missing Psyche family: collisionally eroded or never formed? Icarus **137**(1), 140–151 (1999)

K. de Kleer, S. Cambioni, M. Shepard, The surface of (16) Psyche from thermal emission and polarization mapping. Planet. Sci. J. **2**, 149 (2021). https://doi.org/10.3847/PSJ/ac01ec

M.C. De Sanctis, J.P. Combe, E. Ammannito, E. Palomba, A. Longobardo, T.B. McCord, S. Marchi, F. Capaccioni, M.T. Capria, D.W. Mittlefehldt, C.M. Pieters, J. Sunshine, F. Tosi, F. Zambon, F. Carraro, S. Fonte, A. Frigeri, G. Magni, C.A. Raymond, C.T. Russell, D. Turrini, Detection of widespread hydrated materials on Vesta by the VIR imaging spectrometer on board the Dawn mission. Astrophys. J. **758**, L36 (2012). https://doi.org/10.1088/2041-8205/758/2/l36

B.W. Denevi, D.T. Blewett, D.L. Buczkowski, F. Capaccioni, M.T. Capria, M.C. De Sanctis, W.B. Garry, R.W. Gaskell, L. Le Corre, J.-Y. Li, S. Marchi, T.J. McCoy, A. Nathues, D.P. O'Brien, N.E. Petro, C.M. Pieters, F. Preusker, C.A. Raymond, V. Reddy, C.T. Russell, P. Schenk, J.E.C. Scully, J.M. Sunshine, F. Tosi, D.A. Williams, D. Wyrick, Pitted terrain on Vesta and implications for the presence of volatiles. Science **338**, 246–249 (2012). https://doi.org/10.1126/science.1225374

Elkins-Tanton et al. (2021). This book

L.T. Elkins-Tanton, E. Asphaug, J.F. Bell, H. Bercovici, B. Bills, R. Binzel, W.F. Bottke, S. Dibb, D.J. Lawrence, S. Marchi, T.J. McCoy, R. Oran, R.S. Park, P.N. Peplowski, C.A. Polanskey, T.H. Prettyman, C.T. Russell, L. Schaefer, B.P. Weiss, M.A. Wieczorek, D.A. Williams, M.T. Zuber, Observations, meteorites, and models: a preflight assessment of the composition and formation of (16) Psyche. J. Geophys. Res., Planets **125**, e2019JE006296 (2020). https://doi.org/10.1029/2019JE006296

M. Ferrais, P. Vernazza, L. Jorda, N. Rambaux, J. Hanuš, B. Carry, F. Marchis, M. Marsset, M. Viikinkoski, M. Brož, R. Fetick, A. Drouard, T. Fusco, M. Birlan, E. Podlewska-Gaca, E. Jehin, P. Bartczak, J. Berthier, J. Castillo-Rogez, F. Cipriani, F. Colas, G. Dudziński, C. Dumas, J. Ďurech, M. Kaasalainen, A. Kryszczynska, P. Lamy, H. Le Coroller, A. Marciniak, T. Michalowski, P. Michel, T. Santana-Ros, P. Tanga, F. Vachier, A. Vigan, O. Witasse, B. Yang, Asteroid (16) Psyche's primordial shape: a possible Jacobi ellipsoid. Astron. Astrophys. **638**, L15 (2020). https://doi.org/10.1051/0004-6361/202038100

S. Fornasier, B.E. Clark, E. Dotto, A. Migliorini, M. Ockert-Bell, M.A. Barucci, Spectroscopic survey of M-type asteroids. Icarus **210**, 655–673 (2010)

R.R. Fu, A.I. Ermakov, S. Marchi, J.C. Castillo-Rogez, C.A. Raymond, B.H. Hager et al., The interior structure of Ceres as revealed by surface topography. Earth Planet. Sci. Lett. **476**, 153–164 (2017). https://doi.org/10.1016/j.epsl.2017.07.053

W.B. Garry, D.A. Williams, R.A. Yingst, S.C. Mest, D.L. Buczkowski, F. Tosi, M. Schäfer, L. Le Corre, V. Reddy, R. Jaumann, C.M. Pieters, C.T. Russell, C.A. Raymond, Geologic mapping of ejecta deposits in Oppia Quadrangle, Asteroid (4) Vesta. Icarus **244**, 104–119 (2014)

J. Gattacceca, M. Boustie, L. Hood, J.-P. Cuq-Lelandais, M. Fuller, N.S. Bezaeva, T. de Resseguier, L. Berthe, Can the lunar crust be magnetized by shock: experimental groundtruth. Earth Planet. Sci. Lett. **299**, 42–53 (2010). https://doi.org/10.1016/j.epsl.2010.08.011

P.S. Hardersen, E.A. Cloutis, V. Reddy, T. Mothé-Diniz, J.P. Emery, The M-/X-asteroid menagerie: results of an NIR spectral survey of 45 main-belt asteroids. Meteorit. Planet. Sci. **46**, 1910–1938 (2011)

K.A. Holsapple, K.R. Housen, A crater and its ejecta: an interpretation of deep impact. Icarus **191**(2), 586–597 (2007). https://doi.org/10.1016/j.icarus.2006.08.029

K.A. Holsapple, K.R. Housen, The catastrophic disruptions of asteroids: history, features, new constraints and interpretations. Planet. Space Sci. **179**, 104724 (2019)

L.L. Hood, N.A. Artemieva, Antipodal effects of lunar basin-forming impacts: initial 3D simulations and comparisons with observations. Icarus **193**(2), 485–502 (2008)

Jaumann et al. (2021). This book

R. Jaumann, D.A. Williams, D.L. Buczkowski, R.A. Yingst, F. Preusker, H. Hiesinger, N. Schmedemann, T. Kneissl, J.B. Vincent, D.T. Blewett, B.J. Buratti, U. Carsenty, B.W. Denevi, M.C. De Sanctis, W.B. Garry, H.U. Keller, E. Kersten, K. Krohn, J.-Y. Li, S. Marchi, K.D. Matz, T.B. McCord, H.Y. McSween, S.C. Mest, D.W. Mittlefehldt, S. Mottola, A. Nathues, G. Neukum, D.P. O'Brien, C.M. Pieters, T.H. Prettyman, C.A. Raymond, T. Roatsch, C.T. Russell, P. Schenk, B.E. Schmidt, F. Scholten, K. Stephan, M.V. Sykes, P. Tricarico, R. Wagner, M.T. Zuber, H. Sierks, Vesta's shape and morphology. Science **336**, 687–690 (2012). https://doi.org/10.1126/science.1219122

M. Jutzi, E. Asphaug, The shape and structure of cometary nuclei as a result of low-velocity accretion. Science **348**(6241), 1355–1358 (2015)

M. Jutzi, E. Asphaug, P. Gillet et al., The structure of the asteroid 4 Vesta as revealed by models of planet-scale collisions. Nature **494**, 207–210 (2013). https://doi.org/10.1038/nature11892

K. Krohn, R. Jaumann, D. Elbeshausen, T. Kneissl, N. Schmedemann, R. Wagner, J. Voigt, K. Otto, K.D. Matz, F. Preusker, T. Roatsch, K. Stephan, C.A. Raymond, C.T. Russell, Asymmetric craters on Vesta: impact on sloping surfaces. Planet. Space Sci. **103**, 36–56 (2014)

M. Kueppers, R. Moissl, J.-B. Vincent, S. Besse, S.F. Hviid, B. Carry, B. Grieger, H. Sierks, H.U. Keller, S. Marchi (the OSIRIS Team), Boulders on Lutetia. Planet. Space Sci. **66**, 71–78 (2012)

Lawrence et al. (2021). This book

G. Libourel, A.M. Nakamura, P. Beck, S. Potin, C. Ganino, S. Jacomet et al., Hypervelocity impacts as a source of deceiving surface signatures on iron-rich asteroids. Sci. Adv. **5**, eaav3971 (2019)

K.M. Luchsinger, N.J. Chanover, P.D. Strycker, Water within a permanently shadowed lunar crater: further LCROSS modeling and analysis. Icarus **354**, 114089 (2021)

S. Marchi, M. Massironi, J.-B. Vincent, A. Morbidelli, S. Mottola, F. Marzari, M. Küppers, S. Besse, N. Thomas, C. Barbieri, G. Naletto, H. Sierks, The cratering history of asteroid (21) Lutetia. Planet. Space Sci. **66**, 87–95 (2012a). https://doi.org/10.1016/j.pss.2011.10.010

S. Marchi, H.Y. McSween, D.P. O'Brien, P. Schenk, M.C. De Sanctis, R. Gaskell, R. Jaumann, S. Mottola, F. Preusker, C.A. Raymond, T. Roatsch, C.T. Russell, The violent collisional history of asteroid 4 Vesta. Science **336**, 690–694 (2012b). https://doi.org/10.1126/science.1218757

S. Marchi, W.F. Bottke, D.P. O'Brien, P. Schenk, S. Mottola, M.C. De Sanctis, D.A. Kring, D.A. Williams, C.A. Raymond, C.T. Russell, Small crater populations on Vesta. Planet. Space Sci. **103**, 96–103 (2014). https://doi.org/10.1016/j.pss.2013.05.005

S. Marchi, C.R. Chapman, O.S. Barnouin, J.E. Richardson, J.-B. Vincent, Cratering on asteroids, in *Asteroids IV*, ed. by P. Michel, F.E. DeMeo, W.F. Bottke (University of Arizona Press, Tucson, 2015), pp. 725–744. 895 pp. ISBN 978-0-816-53213-1

S. Marchi, A.I. Ermakov, C.A. Raymond, R.R. Fu, D.P. O'Brien, M.T. Bland, E. Ammannito, M.C. de Sanctis, T. Bowling, P. Schenk, J.E.C. Scully, D.L. Buczkowski, D.A. Williams, H. Hiesinger, C.T. Russell, The missing large impact craters on Ceres. Nat. Commun. **7**, 12257 (2016)

S. Marchi, A. Raponi, T.H. Prettyman, M.C. De Sanctis, J. Castillo-Rogez, C.A. Raymond, E. Ammannito, T. Bowling, M. Ciarniello, H. Kaplan, E. Palomba, C.T. Russell, V. Vinogradoff, N. Yamashita, An aqueously altered carbon-rich Ceres. Nat. Astron. **3**, 140–145 (2019). https://doi.org/10.1038/s41550-018-0656-0

S. Marchi, D.D. Durda, C.A. Polanskey, E. Asphaug, W.F. Bottke, L.T. Elkins-Tanton, L.A.J. Garvie, S. Ray, S. Chocron, D.A. Williams, Hypervelocity impact experiments in iron-nickel ingots and iron meteorites: implications for the NASA Psyche mission. J. Geophys. Res., Planets **125**(2), e05927 (2020)

M. Marsset, M. Brož, P. Vernazza et al., The violent collisional history of aqueously evolved (2) Pallas. Nat. Astron. **4**, 569–576 (2020). https://doi.org/10.1038/s41550-019-1007-5

N. Masoumzadeh, H. Boehnhardt, Global spectrophotometric properties of Asteroid (21) Lutetia using Rosetta-OSIRIS images. Icarus **326**, 1–9 (2019)

M. Massironi, S. Marchi, M. Pajola et al., Geological map and stratigraphy of asteroid (21) Lutetia. Planet. Space Sci. **66**, 125–136 (2012)

T.B. McCord, J.B. Adams, T.V. Johnson, Asteroid Vesta: spectral reflectivity and compositional implications. Science **168**, 1445–1447 (1970). https://doi.org/10.1126/science.168.3938.1445

T.B. McCord, J.Y. Li, J.P. Combe, H.Y. McSween, R. Jaumann, V. Reddy, F. Tosi, D.A. Williams, D.T. Blewett, D. Turrini, E. Palomba, C.M. Pieters, M.C. De Sanctis, E. Ammannito, M.T. Capria, L. Le Corre, A. Longobardo, A. Nathues, D.W. Mittlefehldt, S.E. Schröder, H. Hiesinger, A.W. Beck, F. Capaccioni, U. Carsenty, H.U. Keller, B.W. Denevi, J.M. Sunshine, C.A. Raymond, C.T. Russell, Dark material on Vesta from the infall of carbonaceous volatile-rich material. Nature **491**, 83 (2012). https://doi.org/10.1038/nature11561

H.Y. McSween, R.P. Binzel, M.C. De Sanctis, E. Ammannito, T.H. Prettyman, A.W. Beck, V. Reddy, L. Le Corre, M.J. Gaffey, T.B. McCord, C.A. Raymond, C.T. Russell, Dawn; the Vesta-HED connection; and the geologic context for eucrites, diogenites, and howardites. Meteorit. Planet. Sci. **48**, 2090–2104 (2013). https://doi.org/10.1111/maps.12108

D.A. Minton, C.I. Fassett, M. Hirabayashi, B.A. Howl, J.E. Richardson, The equilibrium size-frequency distribution of small craters reveals the effects of distal ejecta on lunar landscape morphology. Icarus **326**, 63–87 (2019). https://doi.org/10.1016/j.icarus.2019.02.021

A.R. Muxworthy, P.A. Bland, T.M. Davison, J. Moore, G.S. Collins, F.J. Ciesla, Evidence for an impact-induced magnetic fabric in Allende, and exogenous alternatives to the core dynamo theory for Allende magnetization. Meteorit. Planet. Sci. **52**, 2132–2146 (2017)

D. O'Brien, R. Greenberg, J. Richardson, Craters on asteroids: reconciling diverse impact records with a common impacting population. Icarus **183**, 79–92 (2006). https://doi.org/10.1016/j.icarus.2006.02.008

M.E. Ockert-Bell, B.E. Clark, M.K. Shepard, R.A. Isaacs, E.A. Cloutis, S. Fornasier, S.J. Bus, The composition of M-type asteroids: synthesis of spectroscopic and radar observations. Icarus **210**, 674–692 (2010)

R. Oran, B.P. Weiss, Y. Shprits, K. Miljković, G. Tóth, Was the moon magnetized by impact plasmas? Sci. Adv. **6**(40), eabb1475 (2020)

K.A. Otto, S. Marchi, A. Trowbridge, H.J. Melosh, H.G. Sizemore, Ceres crater degradation inferred from concentric fracturing. J. Geophys. Res., Planets **124**, 1188–1203 (2019). https://doi.org/10.1029/2018JE005660

R.S. Park et al., High-resolution shape model of Ceres from stereophotoclinometry using Dawn Imaging Data. Icarus **319**, 812–827 (2019). https://doi.org/10.1016/j.icarus.2018.10.024

R.S. Park et al., Evidence of non-uniform crust of Ceres from Dawn's high-resolution gravity data. Nat. Astron. **4**, 748–755 (2020). https://doi.org/10.1038/s41550-020-1019-1

C.M. Pieters, E. Ammannito, D.T. Blewett, B.W. Denevi, M.C. De Sanctis, M.J. Gaffey, L. Le Corre, J.-Y. Li, S. Marchi, T.B. McCord, L.A. McFadden, D.W. Mittlefehldt, A. Nathues, E. Palmer, V. Reddy, C.A. Raymond, C.T. Russell, Distinctive space weathering on Vesta from regolith mixing processes. Nature **491**, 79–82 (2012). https://doi.org/10.1038/nature11534

Polanskey et al. (2021). This book

T.H. Prettyman, D.W. Mittlefehldt, N. Yamashita, D.J. Lawrence, A.W. Beck, W.C. Feldman, T.J. McCoy, H.Y. McSween, M.J. Toplis, T.N. Titus, P. Tricarico, R.C. Reedy, J.S. Hendricks, O. Forni, L. Le Corre, J.Y. Li, H. Mizzon, V. Reddy, C.A. Raymond, C.T. Russell, Elemental mapping by Dawn reveals exogenic H in Vesta's regolith. Science **338**, 242–246 (2012). https://doi.org/10.1126/science.1225354

T.H. Prettyman, D.W. Mittlefehldt, N. Yamashita, A.W. Beck, W.C. Feldman, J.S. Hendricks, D.J. Lawrence, T.J. McCoy, H.Y. McSween, P.N. Peplowski, R.C. Reedy, M.J. Toplis, L. Le Corre, H. Mizzon, V. Reddy, T.N. Titus, C.A. Raymond, C.T. Russell, Neutron absorption constraints on the composition of 4 Vesta. Meteorit. Planet. Sci. **48**, 2211–2236 (2013). https://doi.org/10.1111/maps.12244

L. Prockter, P. Thomas, M. Robinson, J. Joseph, A. Milne, B. Bussey, J. Veverka, A. Cheng, Surface expressions of structural features on Eros. Icarus **155**, 75–93 (2002). https://doi.org/10.1006/icar.2001.6770

V. Reddy, L. Le Corre, D.P. O'Brien, A. Nathues, E.A. Cloutis, D.D. Durda, W.F. Bottke, M.U. Bhatt, D. Nesvorny, D. Buczkowski, J.E.C. Scully, E.M. Palmer, H. Sierks, P.J. Mann, K.J. Becker, A.W. Beck, D. Mittlefehldt, J.-Y. Li, R. Gaskell, C.T. Russell, M.J. Gaffey, H.Y. McSween, T.B. McCord, J.-P. Combe, D. Blewett, Delivery of dark material to Vesta via carbonaceous chondritic impacts. Icarus **221**, 544–559 (2012). https://doi.org/10.1016/j.icarus.2012.08.011

J.E. Richardson, Cratering saturation and equilibrium: a new model looks at an old problem. Icarus **204**, 697–715 (2009)

M. Robinson, P. Thomas, J. Veverka et al., The nature of ponded deposits on Eros. Nature **413**, 396–400 (2001). https://doi.org/10.1038/35096518

C.T. Russell, C.A. Raymond, A. Coradini, H.Y. McSween, M.T. Zuber, A. Nathues, M.C. De Sanctis, R. Jaumann, A.S. Konopliv, F. Preusker, S.W. Asmar, R.S. Park, R. Gaskell, H.U. Keller, S. Mottola, T. Roatsch, J.E.C. Scully, D.E. Smith, P. Tricarico, M.J. Toplis, U.R. Christensen, W.C. Feldman, D.J. Lawrence, T.J. McCoy, T.H. Prettyman, R.C. Reedy, M.E. Sykes, T.N. Titus, Dawn at Vesta: testing the protoplanetary paradigm. Science **336**, 684–686 (2012). https://doi.org/10.1126/science.1219381

C.T. Russell, C.A. Raymond, E. Ammannito, D.L. Buczkowski, M.C. De Sanctis, H. Hiesinger, R. Jaumann, A.S. Konopliv, H.Y. McSween, A. Nathues, R.S. Park, C.M. Pieters, T.H. Prettyman, T.B. McCord, L.A. McFadden, S. Mottola, M.T. Zuber, S.P. Joy, C. Polanskey, M.D. Rayman, J.C. Castillo-Rogez, P.J. Chi, J.P. Combe, A. Ermakov, R.R. Fu, M. Hoffmann, Y.D. Jia, S.D. King, D.J. Lawrence, J.-Y. Li, S. Marchi, F. Preusker, T. Roatsch, O. Ruesch, P. Schenk, M.N. Villarreal, N. Yamashita, Dawn arrives at Ceres: exploration of a small, volatile-rich world. Science **353**, 1008–1010 (2016). https://doi.org/10.1126/science.aaf4219

P. Schenk, D.P. O'Brien, S. Marchi, R. Gaskell, F. Preusker, T. Roatsch, R. Jaumann, D. Buczkowski, T. McCord, H.Y. McSween, D. Williams, A. Yingst, C. Raymond, C. Russell, The geologically recent giant impact basins at Vesta's South pole. Science **336**, 694–697 (2012). https://doi.org/10.1126/science.1223272

P. Schenk, J. Castillo-Rogez, K.A. Otto, S. Marchi, D. O'Brien, M. Bland, K. Hughson, B. Schmidt, J. Scully, D. Buczkowski, K. Krohn, T. Hoogenboom, G. Kramer, V. Bray, A. Neesemann, H. Hiesinger, T. Platz, M.C. De Sanctis, S. Schroeder, L. Le Corre, L. McFadden, M. Sykes, C. Raymond, C.T. Russell, Compositional control on impact crater formation on mid-sized planetary bodies: dawn at Ceres and Vesta, Cassini at Saturn. Icarus **359**, 114343 (2021a). https://doi.org/10.1016/j.icarus.2021.114343

P.M. Schenk, A. Neesemann, S. Marchi, K. Otto, T. Hoogenboom, D.P. O'Brien, J. Castillo-Rogez, C.A. Raymond, C.T. Russell, G. Osinski, A young age of formation of Rheasilvia basin on Vesta from floor deformation patterns and crater counts. Meteorit. Planet. Sci. **57**, 22–47 (2021b). https://doi.org/10.1111/maps.13772

M.K. Shepard et al., Radar observations and shape model of asteroid 16 Psyche. Icarus **281**, 388–403 (2017)

M.K. Shepard, K. de Kleer, S. Cambioni, P.A. Taylor, A.K. Virkki, E.G. Rívera-Valentin, C. Rodriguez Sanchez-Vahamonde, L. Fernanda Zambrano-Marin, C. Magri, D. Dunham, J. Moore, M. Camarca, Asteroid 16 Psyche: shape, features, and global map. Planet. Sci. J. **2**, 125 (2021). https://doi.org/10.3847/PSJ/abfdba

H. Sierks, P. Lamy, C. Barbieri, D. Koschny, H. Rickman, R. Rodrigo, M.F. A'Hearn, F. Angrilli, M.A. Barucci, J.-L. Bertaux, I. Bertini, S. Besse, B. Carry, G. Cremonese, V. Da Deppo, B. Davidsson, S. Debei, M. De Cecco, J. De Leon, F. Ferri, S. Fornasier, M. Fulle, S.F. Hviid, R.W. Gaskell, O. Groussin, P. Gutierrez, W. Ip, L. Jorda, M. Kaasalainen, H.U. Keller, J. Knollenberg, R. Kramm, E. Kuhrt, M. Kuppers, L. Lara, M. Lazzarin, C. Leyrat, J.J.L. Moreno, S. Magrin, S. Marchi, F. Marzari, M. Massironi, H. Michalik, R. Moissl, G. Naletto, F. Preusker, L. Sabau, W. Sabolo, F. Scholten, C. Snodgrass, N. Thomas, C. Tubiana, P. Vernazza, J.-B. Vincent, K.-P. Wenzel, T. Andert, M. Patzold, B.P. Weiss, Images of asteroid 21 Lutetia: a remnant planetesimal from the early solar system. Science **334**, 487–490 (2011). https://doi.org/10.1126/science.1207325

D. Takir, V. Reddy, J.A. Sanchez, M.K. Shepard, J.P. Emery, Detection of water and/or hydroxyl on asteroid (16) Psyche. Astron. J. **153**, 31 (2016). https://doi.org/10.3847/1538-3881/153/1/31

P. Thomas, Large craters on small objects: occurrence, morphology, and effects. Icarus **142**, 89–96 (1999). https://doi.org/10.1006/icar.1999.6211

P.C. Thomas, L. Prockter, M. Robinson, J. Joseph, J. Veverka, Global structure of asteroid 433 Eros. Geophys. Res. Lett. **29**, 46-1–46-4 (2002). https://doi.org/10.1029/2001GL014599

A.L. Tonge, K.T. Ramesh, O. Barnouin, A model for impact-induced lineament formation and porosity growth on Eros. Icarus **266**, 76–87 (2016). https://doi.org/10.1016/j.icarus.2015.11.018

D. Turrini, J.P. Combe, T.B. McCord, N. Oklay, J.B. Vincent, T.H. Prettyman, H.Y. McSween, G.J. Consolmagno, M.C. De Sanctis, L. Le Corre, A. Longobardo, E. Palomba, C.T. Russell, The contamination of the surface of Vesta by impacts and the delivery of the dark material. Icarus **240**, 86–102 (2014). https://doi.org/10.1016/j.icarus.2014.02.021

P. Vernazza, L. Jorda, B. Carry, J. Hanuš, M. Marsset, M. Viikinkoski, F. Marchis, M. Brož, A. Drouard, T. Fusco, R. Fétick, M. Ferrais (HARISSA team), SPHERE unveils the true face of the largest main belt asteroids. Messenger **179**, 13–16 (2020). https://doi.org/10.18727/0722-6691/5187

M. Viikinkoski, P. Vernazza, J. Hanus, H.L. Coroller, K. Tazhenova, B. Carry, M. Marsset, A. Drouard, F. Marchis, R. Fetick, T. Fusco, J. Durech, M. Birlan, J. Berthier, P. Bartczak, C. Dumas, J. Castillo-Rogez, F. Cipriani, F. Colas, M. Ferrais, J. Grice, E. Jehin, L. Jorda, M. Kaasalainen, A. Kryszczynska, P. Lamy, A. Marciniak, T. Michalowski, P. Michel, M. Pajuelo, E. Podlewska-Gaca, T. Santana-Ros, P. Tanga, F. Vachier, A. Vigan, B. Warner, O. Witasse, B. Yang, (16) Psyche: a mesosiderite-like asteroid? Astron. Astrophys. **619**, L3 (2018). https://doi.org/10.1051/0004-6361/201834091

T.R. Watters, P.C. Thomas, M.S. Robinson, Thrust faults and the near-surface strength of asteroid 433 Eros. Geophys. Res. Lett. **38** (2011). https://doi.org/10.1029/2010GL045302

Weiss et al. (2021). This book

B.P. Weiss, S. Pedersen, I. Garrick-Bethell, S.T. Stewart, K.L. Louzada, A.C. Maloof, N.L. Swanson-Hysell, Paleomagnetism of impact spherules from Lonar crater, India and a test for impact-generated fields. Earth Planet. Sci. Lett. **298**(1–2), 66–76 (2010)

D.A. Williams, B.W. Denevi, D.W. Mittlefehldt, S.C. Mest, P.M. Schenk, R.A. Yingst, D.L. Buczkowski, J.E.C. Scully, W.B. Garry, T.B. McCord, J.-P. Combe, R. Jaumann, C.M. Pieters, A. Nathues, L. Le Corre, M. Hoffmann, V. Reddy, M. Schäfer, T. Roatsch, F. Preusker, S. Marchi, T. Kneissl, N. Schmedemann, G. Neukum, H. Hiesinger, M.C. De Sanctis, E. Ammannito, A. Frigeri, T.H. Prettyman, C.T. Russell, C.A. Raymond, The geology of the Marcia quadrangle of asteroid Vesta: assessing the effects of large, young craters. Icarus **244**, 74–88 (2014a). Special Issue: The Geology of Vesta. https://doi.org/10.1016/j.icarus.2014.01.033

D.A. Williams, R. Jaumann, H.Y. McSween Jr., C.A. Raymond, S. Marchi, N. Schmedemann, C.T. Russell, The chronostratigraphy of protoplanet Vesta. Icarus **244**, 158–165 (2014b). https://doi.org/10.1016/j.icarus.2014.06.027

D.A. Williams, T. Kneissl, A. Neesemann, S.C. Mest, E. Palomba, T. Platz, A. Nathues, A. Longobardo, J.E.C. Scully, A. Ermakov, R. Jaumann, D.L. Buczkowski, M. Schäfer, G. Thangjam, C.M. Pieters, T. Roatsch, F. Preusker, S. Marchi, N. Schmedemann, H. Hiesinger, A. Frigeri, C.A. Raymond, C.T. Russell, The geology of the Kerwan quadrangle of dwarf planet Ceres: investigating Ceres' oldest, largest impact basin. Icarus **316**, 99–113 (2018). The geologic mapping of Ceres. https://doi.org/10.1016/j.icarus.2017.08.015

Zuber et al. (2021). This book